


 Cite this: *RSC Adv.*, 2022, **12**, 10097

## A study on the viscosity reduction mechanism of high-filled silicone potting adhesive by the formation of $\text{Al}_2\text{O}_3$ clusters

Jing Wang, Haihong Ma, Fengmei Ren, Zhengfa Zhou \* and Weibing Xu

Heat dissipation has become a key problem for highly integrated and miniaturized electronic components. High thermal conductivity, good flowability and low coefficient of linear thermal expansion (CLTE) are indispensable performance parameters in the field of electronic potting composite materials. In this study, spherical alumina ( $\text{Al}_2\text{O}_3$ ) was surface modified by  $\gamma$ -(2,3-epoxypropoxy) propyltrimethoxy silane (KH560) and  $\gamma$ -aminopropyltriethoxy silane (KH550) and labelled as  $\text{Al}_2\text{O}_3$ -epoxy and  $\text{Al}_2\text{O}_3$ -NH<sub>2</sub>, respectively.  $\text{Al}_2\text{O}_3$ -epoxy and  $\text{Al}_2\text{O}_3$ -NH<sub>2</sub> powders were equally filled in vinyl silicone oil to prepare a high  $\text{Al}_2\text{O}_3$  loading (89 wt%) precursor of silicone potting adhesive. The viscosity of the precursor rapidly decreased with increasing reaction time of  $\text{Al}_2\text{O}_3$ -epoxy and  $\text{Al}_2\text{O}_3$ -NH<sub>2</sub> at 140 °C. The viscosity reduction mechanism may be due to the formation of some  $\text{Al}_2\text{O}_3$  clusters by the reaction of  $\text{Al}_2\text{O}_3$ -epoxy with  $\text{Al}_2\text{O}_3$ -NH<sub>2</sub>, which results in some vinyl silicone oil segments being held in the channel of particles through capillary phenomenon, leading to the friction among  $\text{Al}_2\text{O}_3$  clusters decreasing considerably. Laser particle size analysis and scanning electron microscopy (SEM) results confirmed the existence of  $\text{Al}_2\text{O}_3$  clusters. Energy dispersive spectroscopy (EDS) and dynamic viscoelasticity experiments revealed that some segments of vinyl silicone oils were held by  $\text{Al}_2\text{O}_3$  clusters. When  $\text{Al}_2\text{O}_3$ -epoxy and  $\text{Al}_2\text{O}_3$ -NH<sub>2</sub> reacted for 4 h, the thermal conductivity, CLTE and volume electrical resistivity of the silicone potting adhesive reached 2.73 W m<sup>-1</sup> k<sup>-1</sup>, 75.8 ppm/°C and 4.6 × 10<sup>13</sup> Ω cm, respectively. A new strategy for preparing electronic potting materials with high thermal conductivity, good flowability and low CLTE is presented.

 Received 29th December 2021  
 Accepted 15th March 2022

DOI: 10.1039/d1ra09417c

[rsc.li/rsc-advances](http://rsc.li/rsc-advances)

### 1. Introduction

The potting operation of electronic devices can not only improve the dust-proof, moisture-proof and anti-vibration performance of devices, but also be conducive to the miniaturization and lightweight of devices.<sup>1</sup> Electronic potting materials usually include epoxy resin (EP), polyurethane, and silicone. Epoxy resin potting adhesive has high hardness, good adhesion, and low CLTE (50–70 ppm/°C),<sup>2</sup> while the repairability of the device is poor.<sup>3,4</sup> Polyurethane potting adhesive has good elasticity and anti-vibration performance, but its thermal resistance is poor (usually lower than 150 °C).<sup>5</sup> Silicone has good elasticity, wide working temperature range of minus 60 to 200 °C, and excellent repairability of the device.<sup>6–8</sup> As a result, silicone potting adhesive is now used in many electronic devices.

In recent years, electronic devices are developing towards high integration and miniaturization. The heat generated by devices needs to be diffused in time to improve the operation

reliability and service life of devices.<sup>9,10</sup> The thermal conductivity of silicone is low ( $\sim$ 0.2 W m<sup>-1</sup> k<sup>-1</sup>),<sup>11,12</sup> which cannot meet the working requirements of potting materials. Thermally conductive but insulating fillers such as boron nitride (BN),<sup>13,14</sup>  $\text{Al}_2\text{O}_3$ ,<sup>15</sup> aluminum nitride (AlN),<sup>16</sup> and silicon carbide (SiC)<sup>17</sup> are often filled to improve the thermal conductivity of silicone potting adhesive. However, the thermal conductivity of polymer-based composites with fillers is relatively low. Preparation of 3D fillers, filler assembling and orientation can effectively improve the thermal conductivity of polymer composites.<sup>18–21</sup> Li *et al.*<sup>22</sup> used the ice template method to assemble BN nanosheets (BNNSs) and silver nanowires (AgNWs), and the thermal conductivity of the composites reached 1.10 W m<sup>-1</sup> k<sup>-1</sup> when the filler addition was only 5.0 vol%. Yang *et al.*<sup>23</sup> prepared a thermally conductive filler with BN bridging carbon fiber (CF), and a special three-dimensional oriented BN/CF/EP composite material was obtained by the vacuum impregnation method, improving the thermal conductivity to 3.1 W m<sup>-1</sup> k<sup>-1</sup>. Song *et al.*<sup>24</sup> prepared 3D- $\text{Al}_2\text{O}_3$ /silicone rubber (SR) frame by a foaming and vacuum infiltration process, and the thermal conductivity of the composite reached 0.747 W m<sup>-1</sup> k<sup>-1</sup> when the loading amount of  $\text{Al}_2\text{O}_3$  was 32.6 wt%. Liu *et al.*<sup>25</sup> obtained 35 wt% BN/30 wt%

School of Chemistry and Chemical Engineering, Hefei University of Technology, Hefei, 230009, People's Republic of China. E-mail: zhengfazhou@hfut.edu.cn; Tel: +86-551-62901455



$\text{Al}_2\text{O}_3$ /polydimethylsiloxane (PDMS) composite materials through a 3-D printing assisted orientation technology, in which the orientation rate and thermal conductivity reached 90.65% and  $3.64 \text{ W m}^{-1} \text{ k}^{-1}$ , respectively. The CLTE of silicone is usually higher than  $200 \text{ ppm}^{\circ}\text{C}$ .<sup>26</sup> Although 3D fillers, filler orientation and self-assembling can improve the thermal conductivity of silicone composites to a certain extent, the CLTE of these composites are often too large to satisfy the potting requirements of specific electronic devices. Thermally conductive but insulating fillers such as  $\text{Al}_2\text{O}_3$  have low CLTE ( $\sim 6.6 \text{ ppm}^{\circ}\text{C}$ ),<sup>27</sup> which can meet the performance requirements of high thermal conductivity and low CLTE of silicone potting adhesive under the condition of large amount of filling. For example, Fu *et al.*<sup>28</sup> prepared a series of dense boric acid modified BNNSs/EP composites by mechanical ball milling and pressure forming processes; the EP composites with 90 wt% BNNSs achieved the maximum thermal conductivity ( $6.7 \text{ W m}^{-1} \text{ k}^{-1}$ ) and the minimum CLTE ( $4.5 \text{ ppm}^{\circ}\text{C}$ ) at a temperature of  $25^{\circ}\text{C}$ . Unfortunately, high filler loading will inevitably cause a sharp increase in the viscosity of silicone potting adhesive, which makes it impossible to achieve potting under mechanical or artificial conditions.<sup>29</sup>

In this study,  $\text{Al}_2\text{O}_3$ -epoxy and  $\text{Al}_2\text{O}_3\text{-NH}_2$  powders were equally filled in vinyl silicone oil to prepare a high  $\text{Al}_2\text{O}_3$  loading (89 wt%) precursor of silicone potting adhesive. The viscosity of the precursor was greatly reduced through the reaction of  $\text{Al}_2\text{O}_3$ -epoxy and  $\text{Al}_2\text{O}_3\text{-NH}_2$  powders, and a mechanism of viscosity reduction was proposed. The experimental results of laser particle size analysis, SEM, EDS, and dynamic viscoelasticity analysis supported the proposed viscosity reducing mechanism. This study presents a new strategy for preparing electronic potting materials with high thermal conductivity, low viscosity and low CLTE.

## 2. Experimental

### 2.1. Materials

Vinyl silicone oil (50 cp) and hydrogen-containing silicone oil ( $H = 0.8 \text{ wt\%}$ ) were provided by Jiande City Sifco Materials Co., Ltd. (China). Spherical alumina (AX10-32,  $\text{Al}_2\text{O}_3$ ) with a mean particle size of  $8.7 \mu\text{m}$  was supplied by Nippon Steel Corporation (Japan).  $\gamma$ -Aminopropyltrimethoxy silane (KH550) and  $\gamma$ -(2,3-epoxypropoxy) propyltrimethoxy silane (KH560) were purchased from Changzhou Runxiang Chemical Co., Ltd (China) with a purity of 99%. Platinum catalysts (1000 ppm) were obtained from Shanghai Guiyou New Materials Technology Ltd. (China). Absolute ethanol, toluene and tetrahydrofuran (THF) were purchased from Aladdin Industrial Corporation (China). All reagents were used as received without any further purification except vinyl silicone oil.

### 2.2. Surface treatment of $\text{Al}_2\text{O}_3$

$\text{Al}_2\text{O}_3$  powders were modified by 1 wt% KH550 and KH560, respectively. The treatment process was the same as in our previous paper.<sup>30</sup> 8 g KH550 was mixed with water and ethanol (the molar ratio of KH550 to water was 1 : 3, the volume ratio of

KH550 to ethanol was 1 : 1) and hydrolyzed at  $30^{\circ}\text{C}$  for 30 min to prepare KH550 hydrolysate. 800 g  $\text{Al}_2\text{O}_3$  powders were added into the high-speed mixer (SHR-10A, Zhangjiagang Beier Machinery Co., Ltd. China). When the temperature of  $\text{Al}_2\text{O}_3$  powders in the high-speed mixer reached  $110^{\circ}\text{C}$ , KH550 hydrolysate was sprayed and stirred at 1000 rpm for 25 min. The KH550 treated  $\text{Al}_2\text{O}_3$  was washed three times using absolute ethanol to remove the ungrafted KH550, and dried in a vacuum oven at  $105^{\circ}\text{C}$  for 5 h. The preparation of KH560 modified  $\text{Al}_2\text{O}_3$  was the same as above.

### 2.3. Preparation of precursor

The vinyl silicone oil was vacuum dried at  $125^{\circ}\text{C}$  for 3 h to remove volatile matter before using. The mass ratio of  $\text{Al}_2\text{O}_3$ -epoxy and  $\text{Al}_2\text{O}_3\text{-NH}_2$  was set as 1 : 1, and the amount of  $\text{Al}_2\text{O}_3$  in the mixture of surface-treated  $\text{Al}_2\text{O}_3$  and vinyl silicone oil was set as 89 wt%. The mixing process was carried out in a high-speed disperser (JFS-1100A, Laizhou Wankai Machinery Co., Ltd. China) at 2000 rpm for 20 min at  $30^{\circ}\text{C}$  using cooling water, then the mixture was transferred to a three-necked flask with a mechanical stirrer at 600 rpm in an oil bath and reacted at  $140^{\circ}\text{C}$  for 0.5 h, 1 h, 2 h, 3 h, and 4 h, respectively, to prepare the precursor of silicone potting adhesive. The epoxy and amino groups on the surface of  $\text{Al}_2\text{O}_3$  can react to different degrees. The mixture directly coming from the high-speed disperser was indicated as the precursor of 0 h reaction time for comparison.

### 2.4. Preparation of silicone potting adhesive

1000 g precursor was mixed with 1 g platinum catalysts and 2.0 g hydrogen-containing silicone oil, respectively, to prepare the A and B components of silicone potting adhesive.

### 2.5. Characterization

X-ray photoelectron spectroscopy (XPS) was utilized to measure elemental content on the surface of  $\text{Al}_2\text{O}_3$  powders by ESCALAB 250Xi (Thermo Electron Corporation, USA).

Thermogravimetric analysis (TG) was carried out on a TGA8000 analyzer (PerkinElmer, USA) at a heating rate of  $10^{\circ}\text{C min}^{-1}$  under a nitrogen atmosphere from  $25^{\circ}\text{C}$  to  $700^{\circ}\text{C}$ .

Shear viscosity was obtained using the NDJ-97 type rotary viscometer (Shanghai Changji, China) at  $25^{\circ}\text{C}$ . The experiment was repeated three times.

Mastersizer 2000 laser particle size analyzer (Malvern Instruments, UK) was used to detect the particle size distribution. 10 g precursor was added in 100 mL toluene under stirring for 10 min, and allowed to settle naturally; the sediments were then collected. This operation was repeated three times to obtain particle sediments. The particle sediments were dispersed in absolute ethanol for testing, and the concentration of the sediments was 0.09%.

Dynamic viscoelasticity analysis of the precursor was performed using small amplitude oscillatory shear (SAOS) at  $25^{\circ}\text{C}$ , on a Malvern Rheometer (HRNANO 200, UK) equipped with cone-and-plate fixture. The diameter of the cone-and-plate was 20 mm, the inclination angle was  $2^{\circ}$ , and the fixed strain was 1%. Pre-shearing was performed before each dynamic



viscoelasticity experiment to eliminate the shear history of the samples.

Gemini 500 field emission scanning electron microscope (Carl Zeiss, German) was utilized to observe the morphology of  $\text{Al}_2\text{O}_3$  clusters. The washing operation of the precursor was the same as the laser particle size analysis, where the sediments were fully dispersed in 50 mL THF, then a drop was taken and dripped on the copper mesh, and dried at 80 °C for 2 h. Before testing, the samples were treated with gold spraying. The distribution of elements was obtained by a high-resolution field emission scanning electron microscope equipped with energy dispersive spectroscopy (Regulus 8230, Japan), and testing pattern was selected to use high-end plane insertion energy spectrum, to eliminate shooting shadow.

TPS 2500S thermal analyzer (Hot Disk, Sweden) was used to characterize the thermal conductivity of silicone potting composite materials, in which the double helix probe of 4 mm diameter was sandwiched between two lamella samples of 2 mm thickness. The CLTE was measured on a TMA402F3 thermo-mechanical analyzer (NETZSCH, German) from 25 °C to 250 °C at a heating rate of 10 °C min<sup>-1</sup>. ZST-121 volume surface resistivity tester (Beijing Zhonghang Times Instrument Equipment, China) was utilized to determine the volume resistivity, and the diameter and thickness of the sample was 8 mm and 2 mm, respectively. The components A and B of silicone potting adhesive were mixed under equal mass. After complete stirring, the mixture was injected into the mold, and vacuumed to eliminate air bubbles. The mixture was cured at 90 °C for 3 h, and then demolded to obtain thermal and insulating test samples.

### 3. Results and discussion

#### 3.1. Surface treatment of $\text{Al}_2\text{O}_3$ powders

Fig. 1 shows the XPS spectra of  $\text{Al}_2\text{O}_3$ -epoxy,  $\text{Al}_2\text{O}_3-\text{NH}_2$ , and pristine  $\text{Al}_2\text{O}_3$  powders, and the content of Si 2p, C 1s, N 1s, and O 1s are provided in Table 1. The C and Si atom content of

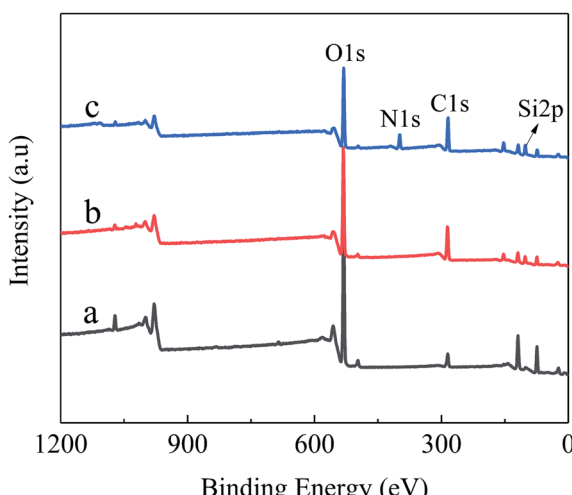


Fig. 1 XPS spectra of powders (a) Pristine  $\text{Al}_2\text{O}_3$ , (b)  $\text{Al}_2\text{O}_3$ -epoxy, (c)  $\text{Al}_2\text{O}_3-\text{NH}_2$ .

Table 1 Element composition on the surface of powders

Sample	Si 2p (%)	C 1s (%)	N 1s (%)	O 1s (%)
Pristine $\text{Al}_2\text{O}_3$	1.85	17.70	0.80	79.65
$\text{Al}_2\text{O}_3$ -epoxy	8.08	42.64	0	49.28
$\text{Al}_2\text{O}_3-\text{NH}_2$	11.46	40.08	10.50	37.96

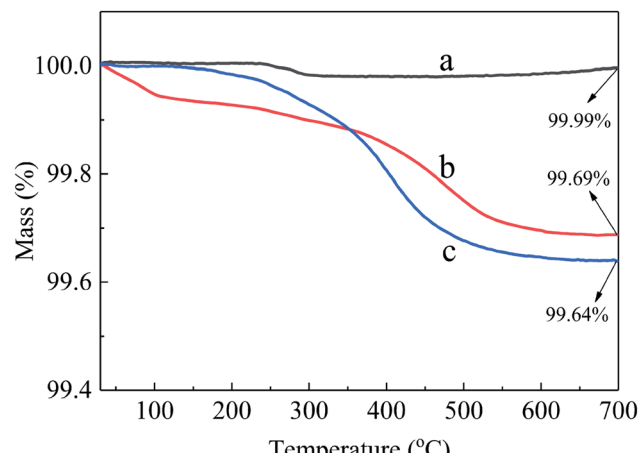


Fig. 2 TG curves of powders (a) pristine  $\text{Al}_2\text{O}_3$ , (b)  $\text{Al}_2\text{O}_3$ -epoxy, (c)  $\text{Al}_2\text{O}_3-\text{NH}_2$ .

$\text{Al}_2\text{O}_3$ -epoxy and  $\text{Al}_2\text{O}_3-\text{NH}_2$  was higher than that of pristine  $\text{Al}_2\text{O}_3$  powders, while the oxygen element content of  $\text{Al}_2\text{O}_3$ -epoxy and  $\text{Al}_2\text{O}_3-\text{NH}_2$  was lower than that of pristine  $\text{Al}_2\text{O}_3$ . The N element content of  $\text{Al}_2\text{O}_3-\text{NH}_2$  was considerably higher than that of pristine  $\text{Al}_2\text{O}_3$ . The results show that KH560 and KH550 are successfully grafted onto the surface of  $\text{Al}_2\text{O}_3$  powders, respectively.<sup>31</sup>

Fig. 2 shows the TG curves of pristine and modified  $\text{Al}_2\text{O}_3$ . The mass retention rate (at 700 °C) of pristine  $\text{Al}_2\text{O}_3$ ,  $\text{Al}_2\text{O}_3$ -epoxy,  $\text{Al}_2\text{O}_3-\text{NH}_2$  was 99.99%, 99.69%, and 99.64%, respectively. The mass loss of pristine  $\text{Al}_2\text{O}_3$  came from the decomposition of the surface free hydroxyl group at high temperature, whereas the weight loss of  $\text{Al}_2\text{O}_3$ -epoxy and  $\text{Al}_2\text{O}_3-\text{NH}_2$  came from the decomposition of not only the free hydroxyl group but also the organic residues of KH560 or KH550 on the surface of  $\text{Al}_2\text{O}_3$ -epoxy and  $\text{Al}_2\text{O}_3-\text{NH}_2$  powders. The amount of residual silane agent grafted on the surface of inorganic powders can be obtained by comparing the mass retention rate difference between pristine and modified inorganic powders.<sup>32</sup> A drop in the thermogram of  $\text{Al}_2\text{O}_3$ -epoxy at 100 °C (0.05%) might be coming from extraneous water, which should be eliminated while calculating the amount of residual KH560 grafted on the surface of  $\text{Al}_2\text{O}_3$ -epoxy. As a result, the amount of residual KH560 and KH550 grafted on the surface of  $\text{Al}_2\text{O}_3$ -epoxy and  $\text{Al}_2\text{O}_3-\text{NH}_2$  was 0.25% and 0.35%, respectively.

#### 3.2. Effect of reaction time on viscosity

The viscosity of potting adhesive has a great impact on the stable production and performance consistency of electronic devices.<sup>33</sup> Fig. 3 shows the effect of reaction time of  $\text{Al}_2\text{O}_3$ -epoxy



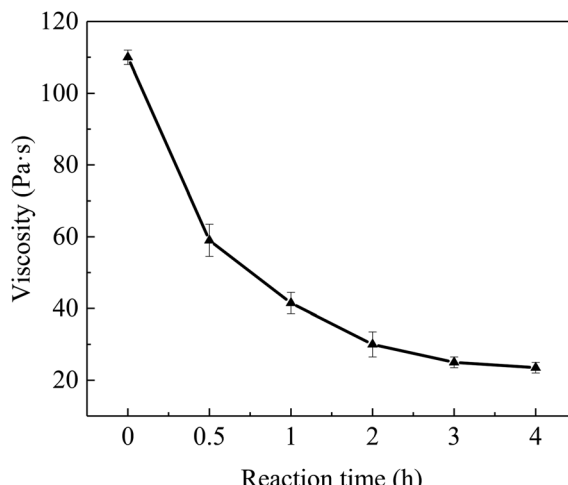


Fig. 3 The viscosity of the mixture versus  $\text{Al}_2\text{O}_3$ -epoxy and  $\text{Al}_2\text{O}_3$ - $\text{NH}_2$  reaction time.

and  $\text{Al}_2\text{O}_3$ - $\text{NH}_2$  at  $140^\circ\text{C}$  on the viscosity of the mixture of vinyl silicone oil filled with surface modified  $\text{Al}_2\text{O}_3$ . The  $\text{Al}_2\text{O}_3$  loading amount was 89 wt%, and the viscosity of the mixture decreased significantly with increasing reaction time. The viscosity reached 110 Pa s when the reaction time was 0 h, and the mixture had difficulty to flow in this state. After  $\text{Al}_2\text{O}_3$ -epoxy and  $\text{Al}_2\text{O}_3$ - $\text{NH}_2$  reacted for 0.5 h, the viscosity of the mixture had dropped about 46.4% of the initial viscosity. The viscosity dropped by 78.6% to 23.5 Pa s when the reaction time was 4 h, and the mixture flowed easily at this point.

It is well known that Richard summarized the effect of particle interaction coefficient ( $\sigma$ ) on the viscosity of the particle filling system.<sup>34</sup> When  $\sigma = 0$ , the suspension viscosity equation was simplified as  $\ln(\eta/\eta_0) = [\eta]\varphi$ , where  $\eta$  is suspension viscosity,  $\eta_0$  and  $[\eta]$  are viscosity and intrinsic viscosity of suspending medium, respectively, and  $\varphi$  is suspension particle volume fraction. For the case  $\sigma = 2$ , the suspension viscosity equation is  $\ln(\eta/\eta_0) = [\eta]\{\varphi/(1 - \varphi/\varphi_n)\}$ , where,  $\varphi_n$  is the maximum particle packing fraction. He concluded that the viscosity of the particle filling mixture increased rapidly with increasing  $\sigma$ . In this work, the  $\varphi$  of  $\text{Al}_2\text{O}_3$  was 0.68. Assuming  $\varphi_n$  was 0.95, when the  $\sigma$  increased from 0 to 2,  $\eta$  would increase  $e^{1.71[\eta]}$  times by the above formula. However, the experimental results showed that the viscosity in this work decreased

significantly with increasing particle interaction. This abnormal phenomenon may be due to the micro aggregation of  $\text{Al}_2\text{O}_3$  particles, which will be discussed later.

### 3.3. Viscosity reduction mechanism

The epoxy groups of  $\text{Al}_2\text{O}_3$ -epoxy can react with the amino groups of  $\text{Al}_2\text{O}_3$ - $\text{NH}_2$  in vinyl silicone oil, resulting in the formation of micro aggregation of  $\text{Al}_2\text{O}_3$  particles as shown in Fig. 4(a). The chemical bond coming from the reaction of the epoxy and amino groups makes  $\text{Al}_2\text{O}_3$  particles contact closely. As a result, tiny pore channels are generated and some vinyl silicone oil segments might immerse in the channels due to capillary phenomenon (Fig. 4(b)). The fixed vinyl silicone oil acts as a lubricator and significantly reduces the friction among  $\text{Al}_2\text{O}_3$  clusters, so the viscosity of the  $\text{Al}_2\text{O}_3$ -epoxy and  $\text{Al}_2\text{O}_3$ - $\text{NH}_2$  reaction system was considerably lower than that of the non-reacting system.

### 3.4. Experimental results supporting the viscosity reduction mechanism

Fig. 5 shows the effect of reaction time of  $\text{Al}_2\text{O}_3$ -epoxy and  $\text{Al}_2\text{O}_3$ - $\text{NH}_2$  at  $140^\circ\text{C}$  on the particle size and particle size distribution of  $\text{Al}_2\text{O}_3$ , and the corresponding data is shown in

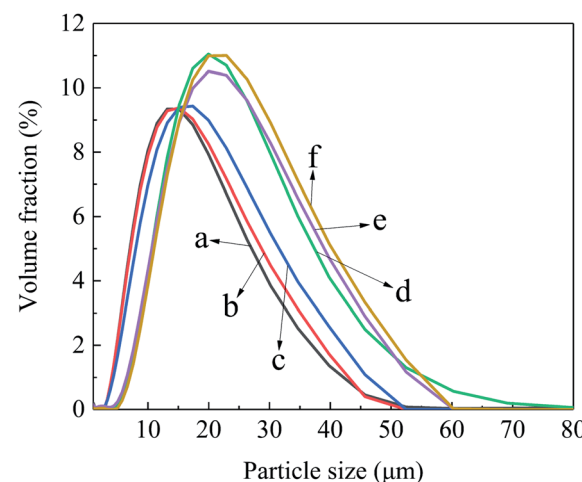


Fig. 5 The particle size distribution curves of  $\text{Al}_2\text{O}_3$  with different reaction time (a) 0 h, (b) 0.5 h, (c) 1 h, (d) 2 h, (e) 3 h, (f) 4 h.

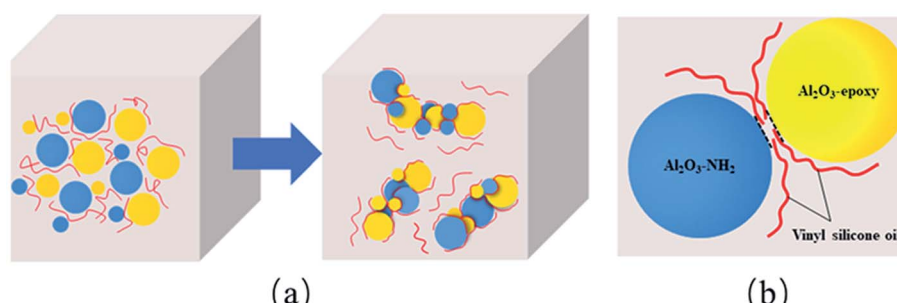


Fig. 4 Diagrams of (a) formation of  $\text{Al}_2\text{O}_3$  clusters, (b) some vinyl silicone oil segments fixing in the interval of particles.



Table 2 The  $D_{10}$ ,  $D_{50}$  and  $D_{90}$  of Fig. 5

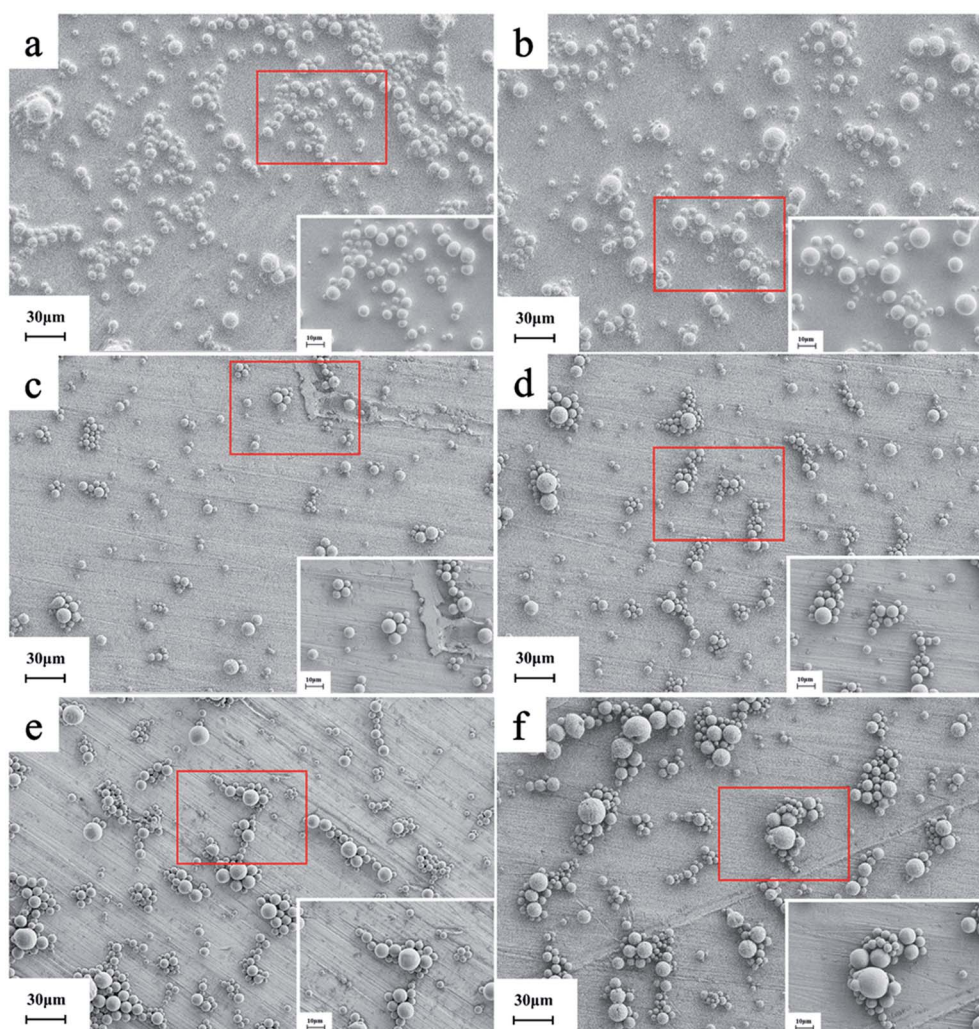
Reaction time/h	$D_{10}/\mu\text{m}$	$D_{50}/\mu\text{m}$	$D_{90}/\mu\text{m}$
0	5.79	12.55	25.21
0.5	6.18	13.07	26.10
1	6.67	14.39	28.31
2	9.53	18.36	33.85
3	8.97	18.35	33.69
4	10.11	19.30	34.71

Table 2. The  $D_{10}$ ,  $D_{50}$  and  $D_{90}$  increased significantly with prolonged reaction time. There was a jump in particle size distribution between 1 h and 2 h reaction times. This phenomenon may be because the degree of epoxy group reacting with the amino group is considerably low at 1 h, but gets much higher at 2 h. The SEM images (Fig. 6) also show that the size of  $\text{Al}_2\text{O}_3$  clusters at 2 h is considerably larger than that at 1 h.

Fig. 6 shows the SEM images of  $\text{Al}_2\text{O}_3$  with  $\text{Al}_2\text{O}_3$ -epoxy and  $\text{Al}_2\text{O}_3-\text{NH}_2$  reacting for different reaction times at 140 °C. It can be seen that the particle distribution was relatively loose when

the reaction time was 0 h (Fig. 6(a)). When epoxy groups reacted with amino for 0.5 h to 1 h, the modified  $\text{Al}_2\text{O}_3$  particles showed slight aggregation and the size of the  $\text{Al}_2\text{O}_3$  clusters was small (Fig. 6(c)). The  $\text{Al}_2\text{O}_3$  clusters became larger at 2 h reaction time, which was consistent with the results of particle size distribution shown in Fig. 5, and the  $\text{Al}_2\text{O}_3$  particles were in close contact with each other (Fig. 6(d)). The size of  $\text{Al}_2\text{O}_3$  clusters was getting larger and larger when the reaction time exceeded 3 h (Fig. 6(e and f)).

Fig. 7 shows the visual element distribution observed by EDS of  $\text{Al}_2\text{O}_3$  with  $\text{Al}_2\text{O}_3$ -epoxy and  $\text{Al}_2\text{O}_3-\text{NH}_2$  reacting for different reaction times. From Fig. 7(a), when the reaction time was 0 h, the images of Al and O elements revealed that the  $\text{Al}_2\text{O}_3$  particles were discrete from each other, and the image of Si element was unclear. Fig. 7(b) and (c) display the Al, O and Si images of  $\text{Al}_2\text{O}_3$  with  $\text{Al}_2\text{O}_3$ -epoxy and  $\text{Al}_2\text{O}_3-\text{NH}_2$  reacting for 1 h and 4 h, respectively. It was found that some  $\text{Al}_2\text{O}_3$  particles contacted tightly, and some Si elements appeared on the surface and interval of  $\text{Al}_2\text{O}_3$  particles. Furthermore, the Si element in Fig. 7(c) was higher and more significant than that in Fig. 7(b) as

Fig. 6 The SEM images of  $\text{Al}_2\text{O}_3$  with different reaction time (a) 0 h, (b) 0.5 h, (c) 1 h, (d) 2 h, (e) 3 h, (f) 4 h.

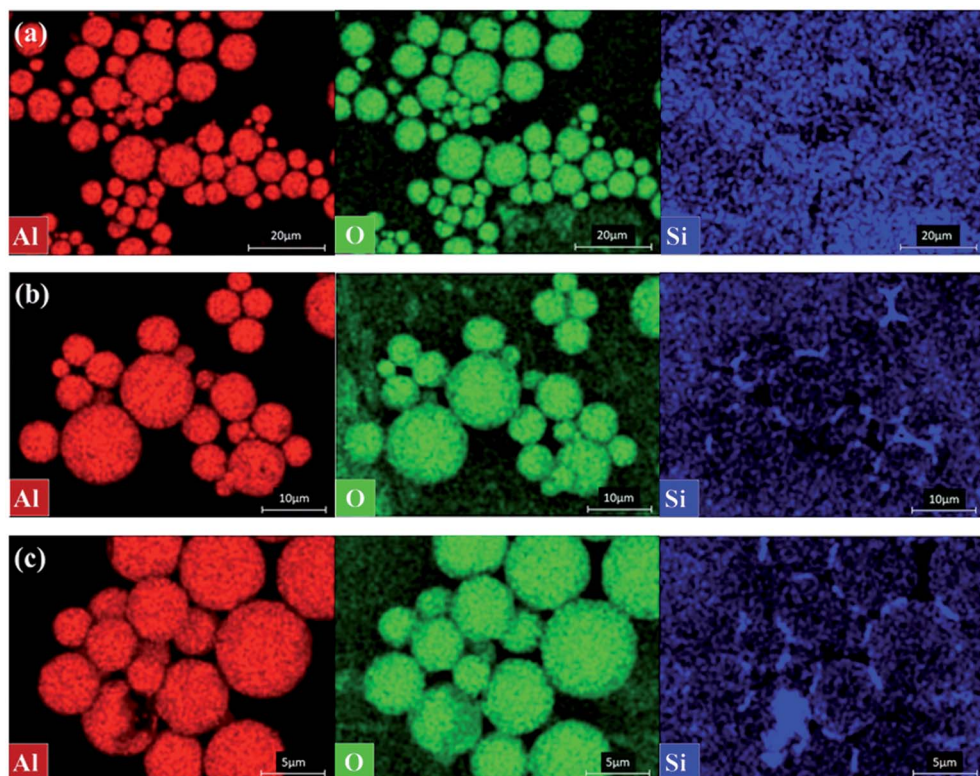


Fig. 7 The Al, O and Si element images of  $\text{Al}_2\text{O}_3$  with different reaction time (a) 0 h, (b) 1 h, (c) 4 h.

the reaction time of  $\text{Al}_2\text{O}_3$ -epoxy and  $\text{Al}_2\text{O}_3$ - $\text{NH}_2$  was prolonged. This phenomenon indicates that some vinyl silicone oil segments are fixed in the intervals of  $\text{Al}_2\text{O}_3$  particles as described in Fig. 4(b).

Fig. 8 shows the dynamic viscoelasticity curves of precursors in which  $\text{Al}_2\text{O}_3$ -epoxy reacts with  $\text{Al}_2\text{O}_3$ - $\text{NH}_2$  for different reaction times. Fig. 8(a) shows the curve of the complex viscosity  $\eta^*$  versus angular frequency  $\omega$ . When the reaction time was 0 h, the precursor exhibited significantly low-frequency shear thinning,<sup>35</sup> while the precursor with powders reacting for 4 h exhibited weak shear thinning at low frequency, and both samples showed shear thickening behavior at high frequency. The change in viscosity is related to a certain structural change inside the liquid. Giuntoli *et al.*<sup>36</sup> studied the  $\alpha$  relaxation kinetic model of a coarse-grained polymer melt under steady-state shear. They found that the shear thinning was due to the action of shearing, the instantaneous combination of macromolecules was “deaggregated” or the fixed particle clusters were destroyed. In this study, when the epoxy and amino groups grafted on the  $\text{Al}_2\text{O}_3$  surface did not undergo a chemical reaction, the  $\text{Al}_2\text{O}_3$  powders were evenly dispersed in the vinyl silicone oil. Only electrostatic interaction, van der Waals forces and solvation exist among modified  $\text{Al}_2\text{O}_3$  powders, and between powders and vinyl silicone oil. Under shear force, the electrostatic attraction, van der Waals forces and solvation were destroyed, and at this moment, the chain of vinyl silicone oil was untangled, resulting in remarkable shear thinning. On the contrary, when the two groups reacted, a chemical bonding

interaction was generated among  $\text{Al}_2\text{O}_3$  powders to form  $\text{Al}_2\text{O}_3$  clusters. A part of the vinyl silicone oil was fixed in the tiny intervals due to capillary phenomenon, which has a lubricating effect resulting in reduced interaction among the  $\text{Al}_2\text{O}_3$  clusters. Hence, the shear thinning phenomenon was weakened.

Fig. 8 (b) and (c) are the curves of the elastic modulus ( $G'$ ) and viscous modulus ( $G''$ ) versus the angular frequency  $\omega$  of precursor with the reaction time of 0 h and 4 h, respectively. It could be clearly seen from the figure that when  $\omega$  was low, the  $G'$  and  $G''$  of the precursor were basically the same at 0 h reaction time. Whereas the  $G''$  was higher than  $G'$  when the reaction time was 4 h. It was because that  $\text{Al}_2\text{O}_3$ -epoxy and  $\text{Al}_2\text{O}_3$ - $\text{NH}_2$  took reaction to build a  $\text{Al}_2\text{O}_3$  cluster structure as shown in Fig. 6. Some segments of vinyl silicone oil were fixed in the particle intervals, which deeply limited the movement ability of the vinyl silicone oil, resulting in its prolonged relaxation time. The relationship between loss factor  $\tan \delta$  and  $\omega$  in Fig. 8(d) further showed that the mechanical loss of the  $\text{Al}_2\text{O}_3$ -epoxy and  $\text{Al}_2\text{O}_3$ - $\text{NH}_2$  reacting system was higher than that of the non-reacting system at lower frequency. As the frequency increased, both  $G'$  and  $G''$  showed an increasing trend, but the increasing speed of  $G'$  exceeded that of  $G''$ . For the non-reacting system, the intersection of  $G'$  and  $G''$  appeared at  $99.58 \text{ rad s}^{-1}$ , while for the 4 h reaction system, the intersection appeared at  $39.64 \text{ rad s}^{-1}$ , indicating that the elastic modulus of the 4 h reaction system is greatly improved. The results may be due to the formation of  $\text{Al}_2\text{O}_3$  clusters in the 4 h reaction system, and  $\text{Al}_2\text{O}_3$  clusters are of a bigger size, which increases the rigidity of the precursor at



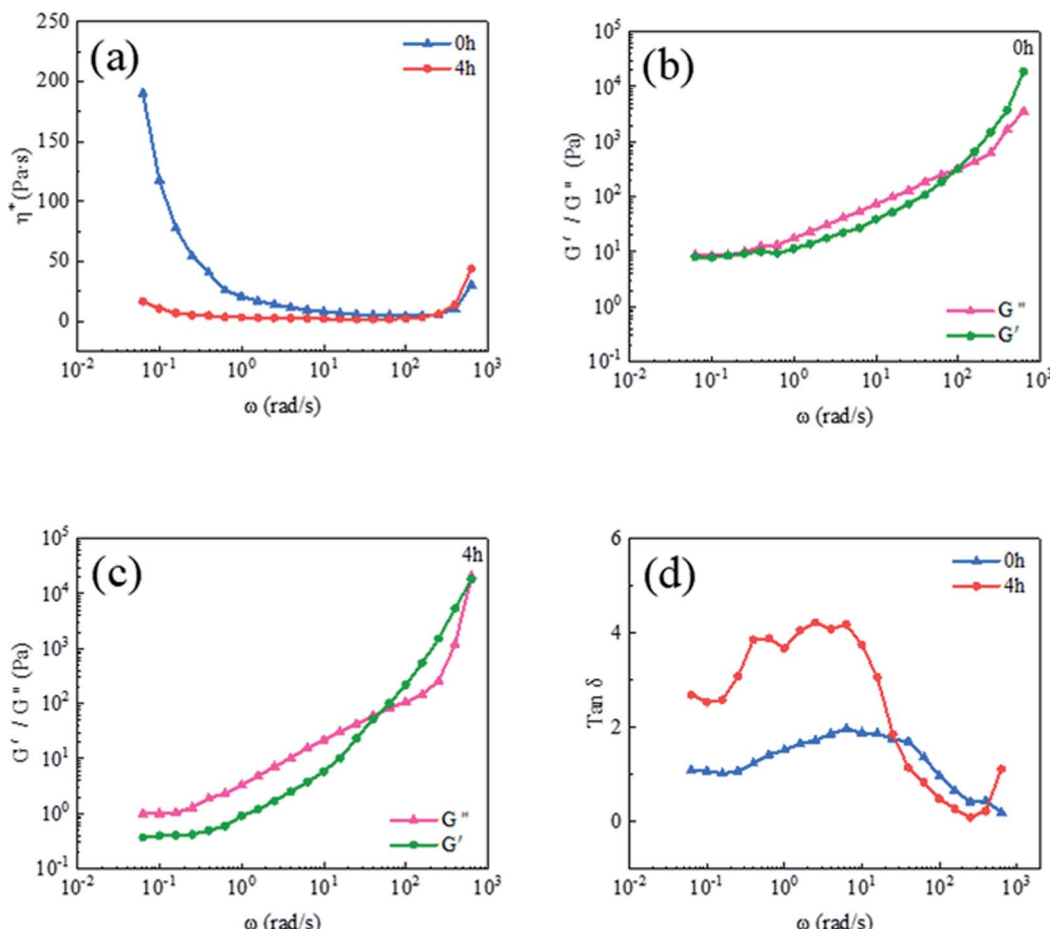


Fig. 8 The dynamic viscoelasticity curves of precursors with different reaction time, (a)  $\eta^*$  versus  $\omega$ , (b) and (c)  $G'$  and  $G''$  versus  $\omega$ , and (d)  $\tan \delta$  versus  $\omega$ .

Table 3 Thermal and insulating properties of silicone potting adhesive

Reaction time (h)	0	0.5	1	2	3	4
Thermal conductivity ( $\text{W m}^{-1} \text{k}^{-1}$ )	2.67	2.69	2.70	2.67	2.71	2.73
CLTE (ppm/ $^{\circ}\text{C}$ )	74.0	73.1	72.4	75.5	74.9	75.8
Volume electrical resistivity ( $\times 10^{13} \Omega \text{ cm}$ )	5.7	4.8	2.5	6.4	7.3	4.6

higher frequency. Zheng *et al.*<sup>37</sup> found that higher  $G'$  depended on larger size and the interaction between aggregations, which is conducive to flocculating a stable 3D network structure.

### 3.5. Thermal and insulating properties

The effect of reaction time of modified  $\text{Al}_2\text{O}_3$  on the performance of silicone potting adhesive is shown in Table 3. The reaction time had little effect on the thermal conductivity, CLTE and the volume electrical resistivity of silicone potting adhesive. In the 4 h reaction system, the thermal conductivity, CLTE and volume electrical resistivity were  $2.73 \text{ W m}^{-1} \text{k}^{-1}$ ,  $75.8 \text{ ppm/}^{\circ}\text{C}$  and  $4.6 \times 10^{13} \Omega \text{ cm}$ , respectively. The viscosity of silicone potting adhesive for the 4 h reaction system was  $19.2 \text{ Pa s}$ , which satisfies the demands of a heat conduction insulation potting material.

## 4. Conclusions

This work found that the viscosity reduction of silicone potting adhesive was related to the formation of filler clusters.  $\text{Al}_2\text{O}_3$ -epoxy and  $\text{Al}_2\text{O}_3\text{-NH}_2$  were successfully obtained by surface silanization. The viscosity of the precursor decreased significantly with an increase in the reaction time of  $\text{Al}_2\text{O}_3$ -epoxy and  $\text{Al}_2\text{O}_3\text{-NH}_2$ . The viscosity of the 4 h reaction system was only 78.6% of 0 h. The reason for this phenomenon might be that chemical bonding interaction among modified  $\text{Al}_2\text{O}_3$  powders promoted the formation of  $\text{Al}_2\text{O}_3$  clusters; some segments of vinyl silicone oils were fixed in tiny particle pore channels through capillary phenomenon, leading to a remarkable lubrication effect of  $\text{Al}_2\text{O}_3$  clusters. Particle size distribution and SEM results revealed the formation of  $\text{Al}_2\text{O}_3$  clusters. EDS

evidently showed the existence of vinyl silicone oil in the particle intervals of clusters. The dynamic viscoelasticity experimental results also supported the assumed viscosity reduction mechanism. Moreover, the as-prepared silicone potting adhesive possessed excellent thermal conductivity, low CLTE and low viscosity.

## Author contributions

Jing Wang: methodology, validation, formal analysis, investigation, data curation, writing – original draft. Haihong Ma: investigation, validation, writing – review & editing. Fengmei Ren: investigation, validation. Zhengfa Zhou: methodology, investigation, validation, writing – review & editing. Weibing Xu: supervision, project administration, funding acquisition.

## Conflicts of interest

There are no conflicts to declare.

## Acknowledgements

The authors are grateful for the support and funding from Anhui Science and Technology Department, China (17030901076).

## References

- 1 S. A. Meguid, C. Zhuo and F. Yang, *J. Electron. Packag.*, 2014, **136**, 041010.
- 2 T. Li, J. Zhang, H. P. Wang, Z. N. Hu and Y. F. Yu, *ACS Appl. Mater. Interfaces*, 2013, **5**, 8968–8981.
- 3 H. Chun, S. Y. Park, S. J. Park and Y. J. Kim, *Polymer*, 2020, **207**, 122916.
- 4 J. C. Foster, C. L. Staiger, J. W. Dugger and E. M. Redline, *ACS Macro Lett.*, 2017, **10**, 940–944.
- 5 N. H. Li, J. P. Liu, X. B. Liu, W. W. Yang, K. P. Song and X. L. Li, *IOP Conf. Ser.: Mater. Sci. Eng.*, 2020, **774**, 012089.
- 6 Y. Xue, X. F. Li, H. S. Wang, F. Zhao, D. H. Zhang and Y. F. Chen, *Mater. Des.*, 2019, **165**, 107580.
- 7 K. P. Ruan, H. Yan, S. J. Zhang, X. T. Shi, Y. Q. Guo and J. W. Gu, *Compos. Sci. Technol.*, 2021, **210**, 108799.
- 8 Y. G. Ouyang, X. F. Li, F. Ding, L. Y. Bai and F. L. Yuan, *Compos. Sci. Technol.*, 2020, **190**, 108019.
- 9 X. T. Yang, C. B. Liang, T. B. Ma, Y. Q. Guo, J. Kong, J. W. Gu, M. J. Chen and J. H. Zhu, *Adv. Compos. Hybrid Mater.*, 2018, **1**, 207–230.
- 10 M. Shtein, R. Nadin, M. Buzaglo and O. Regev, *ACS Appl. Mater. Interfaces*, 2015, **7**, 23725–23730.
- 11 D. Yang, Q. G. Wei, B. Y. Li, L. Y. Yu, Y. F. Ni and L. Q. Zhang, *Composites, Part A*, 2021, **14**, 106260.
- 12 D. Liu, Q. Q. Kong, H. Jia, L. J. Xie, J. P. Chen, Z. C. Tao, Z. Wang, D. Jiang and C. M. Chen, *Carbon*, 2021, **18**, 216–224.
- 13 D. X. Liu, C. G. Ma, H. T. Chi, S. H. Li, P. Zhang and P. B. Dai, *RSC Adv.*, 2020, **10**, 42584–42595.
- 14 C. Y. Xu, M. Miao, X. F. Jiang and X. B. Wang, *Compos. Commun.*, 2018, **10**, 103–109.
- 15 Y. G. Ouyang, L. Y. Bai, H. F. Tian, X. F. Li and F. L. Yuan, *Composites, Part A*, 2022, **152**, 106685.
- 16 Z. L. Wei, W. Q. Xie, B. Z. Ge, Z. J. Zhang, W. L. Yang, H. Y. Xia, B. Wang, H. Y. Jin, N. K. Gao and Z. Q. Shi, *Compos. Sci. Technol.*, 2020, **199**, 108304.
- 17 Y. M. Yao, X. D. Zhu, X. L. Zeng, R. Sun, J. B. Xu and C. P. Wong, *ACS Appl. Mater. Interfaces*, 2018, **10**, 9669–9678.
- 18 H. Y. Chen, V. V. Ginzburg, J. Yang, Y. F. Yang, W. Liu, Y. Huang, L. B. Du and B. Chen, *Prog. Polym. Sci.*, 2016, **59**, 41–85.
- 19 F. Zhang, Y. Y. Feng and W. Feng, *Mater. Sci. Eng. R*, 2020, **142**, 100580.
- 20 X. M. Zhang, J. J. Zhang, L. C. Xia, C. H. Li, J. F. Wang, F. Xu, X. L. Zhang, H. Wu and S. Y. Guo, *ACS Appl. Mater. Interfaces*, 2017, **9**, 22977–22984.
- 21 Y. Hue, H. S. Wang, X. F. Li and Y. F. Chen, *Composites, Part A*, 2021, **144**, 106336.
- 22 H. T. Li, C. J. Fu, N. Chen, T. Zhang, J. M. Liu, G. P. Du, L. L. Ren, X. L. Zeng and R. Sun, *Compos. Commun.*, 2021, **25**, 100601.
- 23 Y. Wang, Y. Gao, B. Tang, X. F. Wu, J. Chen, L. M. Shan, K. Sun, Y. T. Zhao, K. Yang, J. H. Yu and W. G. Li, *RSC Adv.*, 2021, **11**, 25422–25430.
- 24 J. N. Song, L. Wu and Y. Zhang, *Polym. Bull.*, 2020, **77**, 2139–2153.
- 25 M. J. Liu, S. W. Chiang, X. D. Chu, J. Li, L. Gan, Y. B. He, B. H. Li, F. Y. Kang and H. D. Du, *Ceram. Int.*, 2020, **46**, 20810–20818.
- 26 N. Suzuki, S. Kiba, Y. Kamachi, N. Miyamoto and Y. Yamauchi, *J. Mater. Chem.*, 2011, **21**, 5338–5344.
- 27 Y. J. Wan, G. Li, Y. M. Yao, X. L. Zeng, P. L. Zhu and R. Sun, *Compos. Commun.*, 2020, **19**, 154–167.
- 28 K. Fu, J. W. Yang, C. C. Cao, Q. H. Zhai, W. Qiao, J. X. Qiao, H. J. Gao, Z. Zhou, J. W. Ji and M. Y. Li, *ACS Appl. Mater. Interfaces*, 2021, **13**, 2853–2867.
- 29 Y. Hu, C. Chen, Y. F. Wen, Z. G. Xue, X. P. Zhou, D. Shi, G. H. Hu and X. L. Xie, *Compos. Sci. Technol.*, 2021, **209**, 108760.
- 30 F. M. Ren, R. Zhou, F. Sun, H. H. Ma, Z. F. Zhou and W. B. Xu, *RSC Adv.*, 2017, **7**, 29779–29785.
- 31 Q. Guo, P. L. Zhu, G. Li, J. J. Wen, T. Y. Wang, D. Q. Lu, R. Sun and C. P. Wong, *Composites, Part B*, 2017, **116**, 388–397.
- 32 Y. M. Han, J. Y. Zhang, Q. Y. Yang, L. Shi, S. C. Qi and R. G. Jin, *J. Appl. Polym. Sci.*, 2008, **107**, 3788–3795.
- 33 C. Chen, Y. Xue, X. W. Li, Y. F. Wen, J. W. Liu, Z. G. Xue, D. A. Shi, X. P. Zhou, X. L. Xie and Y. W. Mai, *Composites, Part A*, 2019, **118**, 67–74.
- 34 R. D. Sudduth, *J. Appl. Polym.*, 1993, **48**, 37–55.
- 35 J. E. Butler and B. Snook, *Annu. Rev. Fluid. Mech.*, 2018, **50**, 299–318.
- 36 A. Giuntoli, F. Puosi, D. Leporini, F. W. Starr and J. F. Douglas, *Sci. Adv.*, 2020, **6**, eaaz0777.
- 37 Z. Zheng, Y. H. Song, X. Wang and Q. Zheng, *J. Rheol.*, 2015, **59**, 971–993.

